Mixed Valence Triiron Complexes from the Conjugation of [$Fe^{I}Fe^{I}$] and [Fe^{II}] Complexes via Intermolecular Carbyne/Alkyne Coupling

Giulio Bresciani, Gianluca Ciancaleoni, Stefano Zacchini, Lorenzo Biancalana, Guido Pampaloni, Tiziana Funaioli, Fabio Marchetti

The cooperative behavior of a diiron framework facilitated the effortless synthesis of triiron complexes, where the iron centers exist in two different oxidation states, achieved by linking two hydrocarbyl ligands and resulting in an innovative multisite ligand configuration.

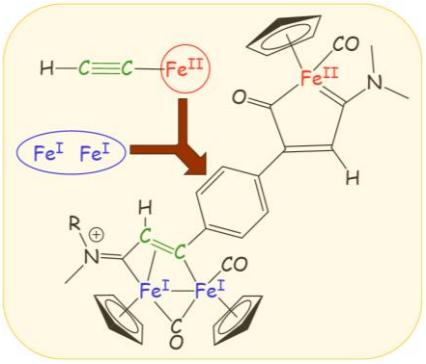

Mixed Valence Triiron Complexes from the Conjugation of [$Fe^{I}Fe^{I}$] and [Fe^{II}] Complexes via Intermolecular Carbyne/Alkyne Coupling

Giulio Bresciani,[a,c,*] Gianluca Ciancaleoni,[a,c] Stefano Zacchini,[b,c] Lorenzo Biancalana,[a,c] Guido Pampaloni,[a,c] Tiziana Funaioli,[a,c,*] Fabio Marchetti [a,c]

[a] University of Pisa, Department of Chemistry and Industrial Chemistry, Via G. Moruzzi 13, I-56124 Pisa, Italy

[b] University of Bologna, Department of Industrial Chemistry "Toso Montanari", Viale Risorgimento 4, I-40136 Bologna, Italy

[c] CIRCC, Via Celso Ulpiani 27, I-70126 Bari, Italy

Corresponding Authors

giulio.bresciani@dcci.unipi.it; tiziana.funaioli@unipi.it

Abstract

We present a new synthetic strategy for obtaining mixed-valence triiron complexes where the metal centers are bridged by a novel, highly functionalized hydrocarbyl ligand. The alkynyl-vinyliminium complexes $[Fe_2Cp_2(CO)(\mu\text{-}CO)\{\mu\text{-}\eta^1\text{:}\eta^3\text{-}C(X\text{-}C{\equiv}CH)CHCNMe_2\}]CF_3SO_3$ (X = 4-C_6H_4, **[2a1]CF_3SO_3**; X = $(CH_2)_3$, **[2a2]CF_3SO_3**) were synthesized in almost quantitative yields from the aminocarbyne precursor $[Fe_2Cp_2(CO)_2(\mu\text{-}CO)\{\mu\text{-}CNMe_2\}]CF_3SO_3$, **[1a]$CF_3SO_3$**, and the di-alkynes HC≡C-X-C≡CH. Then, the ferracycle [Fe(Cp)(CO){C(NMe_2)CH=C(4-C_6H_4C≡CH)C(O)}], **4a1**, was produced in 47% yield from the cleavage of **[2a1]CF_3SO_3** promoted by pyrrolidine. Subsequent reactions of the acetonitrile adducts $[Fe_2Cp_2(CO)(\mu\text{-}CO)(NCMe)\{\mu\text{-}CNMe(R)\}]CF_3SO_3$ (R = Me, **[1a^{ACN}]CF_3SO_3**; R = Xyl, **[1b^{ACN}]CF_3SO_3**) ([Fe^IFe^I]) with **4a1** ([Fe^{II}]) at room temperature resulted in the formation of [$Fe^IFe^IFe^{II}$] complexes $[Fe_2Cp_2(CO)(\mu\text{-}CO)\{\mu\text{-}\eta^1\text{:}\eta^3\text{-}C(X\text{-}C{=}CHC(NMe_2){=}FeCp(CO)C{=}O)CHCNMe(R)\}]CF_3SO_3$ (R = Me, **[5a1]CF_3SO_3**; R = Xyl, **[5b1]CF_3SO_3**) in yields ranging from 56% to 64%. The new products were characterized by IR and multinuclear NMR spectroscopy, and the structures of **[2a2]CF_3SO_3** and **4a1** were confirmed by single crystal X-ray diffraction. Cyclic voltammetry and spectroelectrochemical studies on **[5a1]$^+$** have revealed that reduction and oxidation events occur almost independently at the [Fe^IFe^I] and [Fe^{II}] units, respectively. This observation underscores a minimal interconnection between the two fragments within the triiron complex. Accordingly, DFT studies pointed out that the HOMO and LUMO orbitals are predominantly localized in the two distinct compartments of **[5a1]$^+$**.

Keywords: mixed-valence metal complexes; diiron complexes; alkyne insertion; vinyliminium ligand; electrochemistry

Introduction

The increase in nuclearity within transition metal complexes is of significant interest due to the potential for polynuclear complexes to exhibit enhanced properties compared to their lower nuclearity counterparts.[1,2,3] In this field, mixed-valence metal complexes (MVMCs), comprising two or more metal atoms of the same element but in distinct oxidation states, have garnered considerable attention. In particular, MVMCs serve as excellent templates to elucidate the factors that govern electron-transfer and electron delocalization in metal-ligand assemblies.[4,5,6,7,8]

The synthesis of polynuclear compounds can generally be accomplished through the thermal treatment of well-defined mononuclear precursors,[9,10] or by using suitable bridging ligands as linkers between the metal atoms.[11,12,13,14,15,16]

Another widely employed strategy, for assembling homo- and heteronuclear organometallic compounds, involves coordinating a pendent alkyne group from a monometallic complex to a second metal center or cluster fragment.[17,18,19,20,21] On the other hand, while insertion reactions of alkynes into metal-ligand units are rather common in organometallic chemistry,[22,23,24,25,26,27] the alkyne insertion approach has been barely explored for increasing the nuclearity of metallic structures. A relevant exception regards iron-platinum dimetallacyclopentenone complexes with an alkyne pendant, which was incorporated within a second [FePt] scaffold through insertion into the Pt-(μ-CO) bond.[28]

The demand for the development of sustainable synthetic methodologies makes organo-iron complexes ideal platforms for exploring novel reaction pathways, given the abundance and environmental benignity of iron.[29,30,31,32] The combination of monoiron units using multidentate ligands has been employed to obtain a variety of polyiron species, including Fe_3 and Fe_4 structural motifs.[33,34,35,36] Additionally, mixed-valence triiron carbonyl compounds have aroused a great interest as optimized models for natural [FeFe] hydrogenases, facilitating reversible H_2 formation from proton reduction; these compounds displayed improved performance when compared to related diiron complexes.[37,38] However, the synthetic routes for accessing mixed-valence organo-polyiron structures are not always straightforward, and it is worth noting that certain compounds of

this nature have been obtained through non-reproducible routes.[39] Therefore, the development of a reproducible, safe and easy synthesis of polynuclear iron compounds should be a goal to be pursued.

Diiron complexes have the potential to play a key role in constructing complexes with higher nuclearity. The bimetallic framework indeed promotes cooperative effects that enable unconventional reactivity patterns on the bridging ligands.[40,41,42,43,44,45,46] In this context, the commercially available $[Fe_2Cp_2(CO)_4]$ (Cp = η^5-C_5H_5)[47] represents a convenient and versatile platform for assembling small molecular units, creating a diverse range of hydrocarbyl fragments (Scheme 1).[48,49,50,51] It should be noted that the rich reactivity of derivatives based on the Fe_2Cp_2 core might favor the dimerization to tetrairon structures through the coupling of appropriate functions on the bridging hydrocarbyl ligand. In some cases, these coupling processes are triggered by electron transfer events.[52,53,54]

Based on our longtime experience with bis-cyclopentadienyl [Fe^IFe^I] systems, we present here the development of a novel synthetic strategy of two mixed-valence triiron complexes and their structural and electrochemical characterization. These systems can be prepared at room temperature, free from the use of hazardous chemicals and employing a unique Fe2 + Fe1 assembly method that involves the insertion of an alkyne into the metal-ligand framework. To the best of our knowledge, this approach is rarely documented in the synthesis of polynuclear compounds. Diiron complexes featuring bridging aminocarbyne or vinyliminium ligands (depicted as structures **I** and **II**, respectively, in Figure 1) can be sequentially generated from the readily available $[Fe_2Cp_2(CO)_4]$.[55,49] Vinyliminium complexes **II**, resulting from the coupling of the aminocarbynes with alkynes,[56] form a potentially unlimited family of organometallic compounds, thanks to the wide applicability of the synthetic procedure and also due to their highly diverse chemistry.[55] This array of possibilities enabled the conjugation of a monoiron complex with a diiron structure via an alkyne insertion procedure.

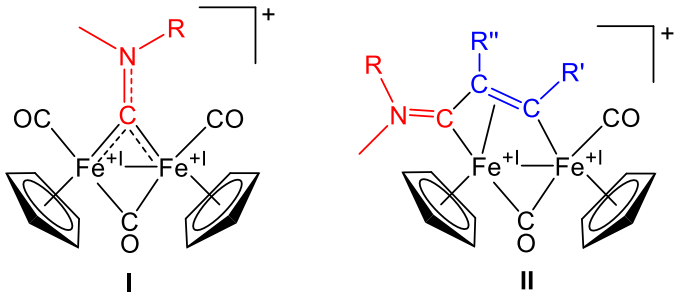

Figure 1. Structures of (**I**) diiron μ-aminocarbyne complexes and (**II**) diiron μ-vinyliminium complexes derived from the coupling of the aminocarbyne ligand (red) with alkynes (blue). R = alkyl or aryl; R′ = alkyl, aryl, H, thiophenyl, pyridyl, silyl, carboxylate; R′′ = H (most frequently), alkyl, Ph, carboxylate.

Results and discussion

Following the well-established general synthetic procedure,[56] we synthesized the novel complexes **[2a1]CF_3SO_3** and **[2a2]CF_3SO_3**, containing an alkynyl-decorated bridging vinyliminium ligand, from the aminocarbyne precursor **[1a]CF_3SO_3** and, respectively, 1,4-diethynylbenzene and 1,6-heptadiyne (Scheme 1). This synthetic route involves the initial displacement of one CO ligand with a labile NCMe molecule (according to the "TMNO strategy" [57,58,59]), followed by acetonitrile-alkyne substitution and subsequent insertion of the alkyne into the iron-carbyne bond. The organic reagents possess two terminal alkyne groups separated by distinct linkers; the synthesis of **[2a1]CF_3SO_3** and **[2a2]CF_3SO_3** proceeded smoothly (90-96% yields), thereby preventing the generation of by-products from potential double alkyne insertion reactions.

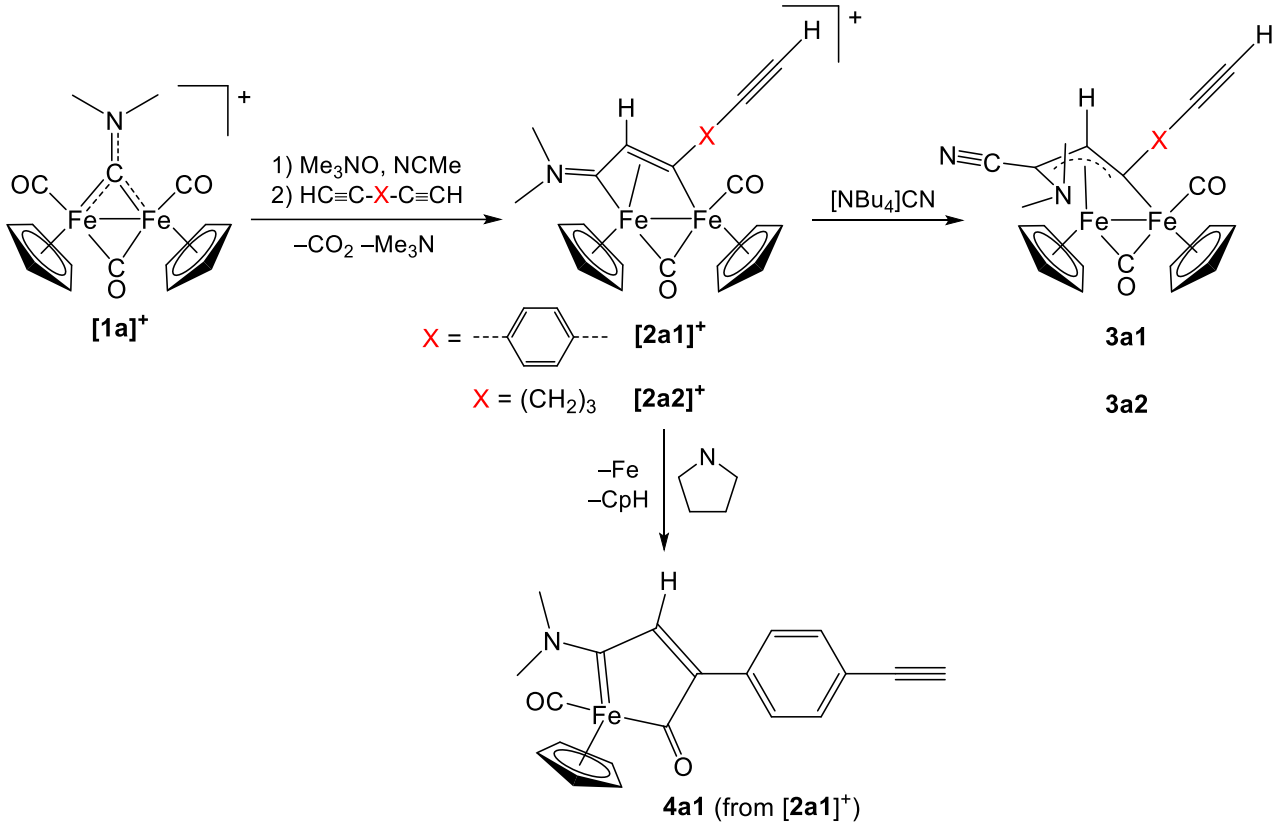

Scheme 1. Synthesis of cationic diiron alkynyl-vinyliminium complexes ([**2a1**]$^+$ / [**2a2**]$^+$, triflate salts) and subsequent modification to neutral diiron cyano-aminoallylidene (**3a1** / **3a2**) and monoiron vinyl-aminoalkylidene (**4a1**) complexes. All reactions were conducted at room temperature.

IR and NMR data of **[2a1]CF$_3$SO$_3$** and **[2a2]CF$_3$SO$_3$** are consistent with literature data on various diiron vinyliminium complexes.[56,60] In the IR spectra (recorded on dichloromethane solutions), a standard pattern is observed with three bands ascribable to the terminal CO, the bridging CO and the iminium moiety (*e.g.*, at 1992, 1808 and 1685 cm^{-1}, respectively, for **[2a1]CF$_3$SO$_3$**). In addition, the alkynyl group exhibits a weak absorption around 2110 cm^{-1}. The ^{1}H NMR spectra (acetone-d$_6$ solutions) show one single set of resonances, where the Cp protons resonate at ca. 5.5 and 5.2 ppm; this indicates that the Cp rings adopt a mutual cis-orientation with respect to the Fe-Fe axis. In fact, trans isomers of diiron vinyliminium complexes, when present, usually display one Cp resonance that is notably upfield shifted (δ < 5.0 ppm).[60]

Distinctive features of the ^{13}C NMR spectra of **[2a1]CF$_3$SO$_3$** and **[2a2]CF$_3$SO$_3$** are given by the resonances of the peripheral carbons of the C$_3$ chain, detected at 225.5 ppm and 202.2 ppm in the

case of **[2a1]CF$_3$SO$_3$**, in alignment with their amino-alkylidene and bridging alkylidene nature, respectively.[61,62] The alkynyl carbons resonate within the range of 71.0 - 85.0 ppm.

The structure of **[2a2]CF$_3$SO$_3$** was confirmed by a single crystal X-ray diffraction study (Figure 2). The bonding parameters and overall geometry of the cation **[2a2]**$^+$ resemble those previously reported for the closely related complex [$Fe_2Cp_2(CO)(\mu\text{-}CO)\{\mu\text{-}\eta^1\text{:}\eta^3\text{-}C(Me)CHCNMe_2\}]^+$.[63]

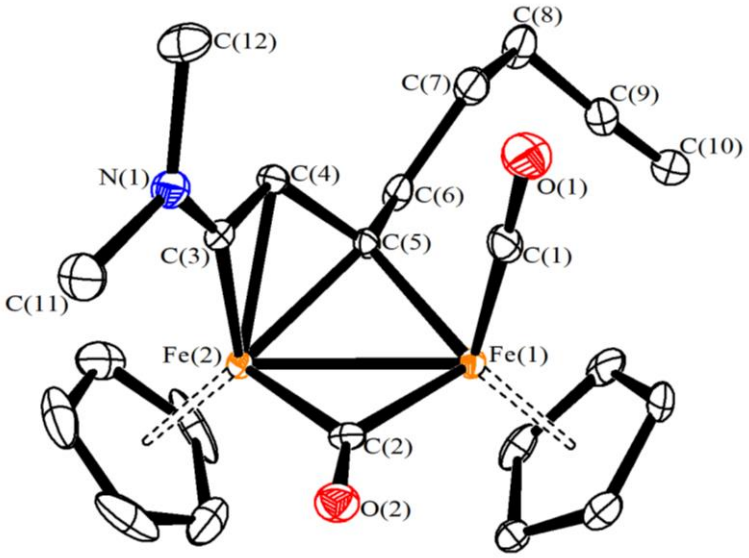

Figure 2. View of the structure of [**2a2**]$^+$. Displacement ellipsoids are at the 30% probability level. H-atoms have been omitted for clarity. Main bond distances (Å) and angles (°): Fe(1)-Fe(2) 2.5349(9), Fe(1)-C(1) 1.753(5), Fe(1)-C(2) 1.903(5), Fe(2)-C(2) 1.938(5), Fe(2)-C(3) 1.841(5), Fe(2)-C(4) 2.049(4), Fe(2)-C(5) 2.029(4), Fe(1)-C(5) 1.950(4), C(1)-O(1) 1.135(6), C(2)-O(2) 1.173(6), C(3)-N(1) 1.282(6), C(3)-C(4) 1.414(6), C(4)-C(5) 1.414(6), C(5)-C(6) 1.518(6), C(6)-C(7) 1.533(7), C(7)-C(8) 1.525(7), C(8)-C(9) 1.465(8), C(9)-C(10) 1.178(8), Fe(1)-C(1)-O(1) 177.5(4), Fe(1)-C(2)-Fe(2) 82.58(18), Fe(1)-C(5)-Fe(2) 79.10(16), C(3)-C(4)-C(5) 116.6(4), C(5)-C(6)-C(7) 108.6(4), C(6)-C(7)-C(8) 114.7(5), C(7)-C(8)-C(9) 113.4(5), C(8)-C(9)-C(10) 176.2(6), sum at N(1) 359.8(7).

With the aim of constructing poly-iron structures, we synthesized and isolated the diiron aminocarbyne acetonitrile adducts **[1a^{ACN}]CF$_3$SO$_3$** and **[1b^{ACN}]CF$_3$SO$_3$** (Scheme 2). When [**1a^{ACN}**]$^+$ was allowed to interact with [**2a1**]$^+$ / [**2a2**]$^+$, the acetonitrile ligand was not displaced by the alkynyl side-function present in the cations even upon prolonged heating in refluxing THF. We speculated that an alkyne within a *neutral* complex, rather than a *cationic* one, could favor the *nucleophilic* substitution of the acetonitrile ligand by the {C≡C} triple bond.

To generate neutral derivatives, **[2a1]CF$_3$SO$_3$** / **[2a2]CF$_3$SO$_3$** were allowed to react with tetrabutylammonium cyanide in dichloromethane, affording the cyano-aminoallylidene products

3a1 / **3a2** in approximately 80% yields (Scheme 1). This reaction mirrors a general process previously documented for complexes lacking alkynyl functionality.[64] Compounds **3a1** / **3a2**, like their cationic precursors, retain a pair of Fe^{I} centers. The synthesis of **3a1** and **3a2** is characterized by regio- and stereo-selectivity, with the cyanide anion adding to the iminium carbon and being finally oriented *syn* with respect to the adjacent CH. In related complexes, this configuration permits a stabilizing intramolecular Lewis acid-base interaction between the amine nitrogen's lone pair and the terminal carbonyl ligand.[64] As a consequence, the $\{NMe_2\}$ unit becomes constrained, leading to non equivalent methyl groups in the NMR spectra [e.g. for **3a1**, $CDCl_3$ solution: $\delta(^1H)$ = 2.35, 1.82 ppm; $\delta(^{13}C)$ = 49.8, 42.1 ppm]. The IR spectra show the absorption attributed to the cyano moiety, at approximately 2190 cm^{-1}, and that of the alkynyl (*e.g.* at 2138 cm^{-1} in **3a2**). The NMR resonance of the alkynyl CH moiety experiences an upfield shift going from [**2a1**]$^+$ / [**2a2**]$^+$ to **3a1** / **3a2** (*e.g.* for **[2a1]**$^+$ and **3a1**, respectively: $\delta(^1H)$ = 3.81 ppm, 3.17 ppm; $\delta(^{13}C)$ = 79.9 ppm, 77.6 ppm).

With **3a1 / 3a2** in hand, we explored their potential reaction with **[1a^{ACN}]CF_3SO_3** and **[1b^{ACN}]CF_3SO_3** at room temperature; however, each combination gave a mixture of products that could not be separated. This outcome might stem from the cyano group within **3a1 / 3a2** competing with the alkynyl pendant for the substitution of the NCMe ligand.[65] Moreover, the conversion did not proceed to completion, probably due to the steric hindrance around the alkyne and cyano moieties within **3a1 / 3a2**.

Therefore, to overcome the observed drawbacks and promote a straightforward intermolecular carbyne/alkyne coupling, we aimed to obtain an alkynyl-functionalized monoiron complex without any additional potentially coordinating group.

Based on the literature, diiron vinyliminium complexes bearing an aryl substituent on the vinyl unit are susceptible to converting into monoiron(II) species comprising the same C_3N chain as in the vinyliminium upon treatment with a mild reducing agent.[66] This reaction typically involves the elimination of atomic iron and cyclopentadiene. In the case of [**2a1**]$^+$, this transformation was

conducted by treating the diiron complex with pyrrolidine in tetrahydrofuran solution, yielding the product **4a1** in a 47% isolated yield. The IR spectrum of **4a1** (CH_2Cl_2 solution) displays absorptions related to the carbonyl ligand (1916 cm^{-1}), the metalla-acyl (1526 cm^{-1}), and the amino-alkylidene functionalities (1602 cm^{-1}). In the NMR spectra, the two N-methyl groups show two resonances (*e.g.*, at 3.74 and 3.55 ppm in the ^1H spectrum), in line with the partial double-bond character of the alkylidene-nitrogen bond.[67] The presence of the alkenyl moiety is evident from the characteristic chemical shifts of the CH unit [$\delta(^1H)$ = 7.66 ppm; $\delta(^{13}C)$ = 146.7 ppm]; these signals are substantially shifted with respect to the corresponding signals in [**2a1**]$^+$ (4.68 and 53.5 ppm, respectively). The Fe-C-N carbon resonates at 262.2 ppm in **4a1**, whereas it occurs at 225.2 ppm in [**2a1**]$^+$, in accord with its increased amino-alkylidene over iminium nature in **4a1**.

The structure of **4a1** was ascertained by X-ray diffraction analysis (Figure 3), which demonstrated its close relation to previously reported five-membered metallacycle complexes.[66] These complexes are composed of fused vinyl-aminoalkylidene (C_3N) and acyl (CO) units.

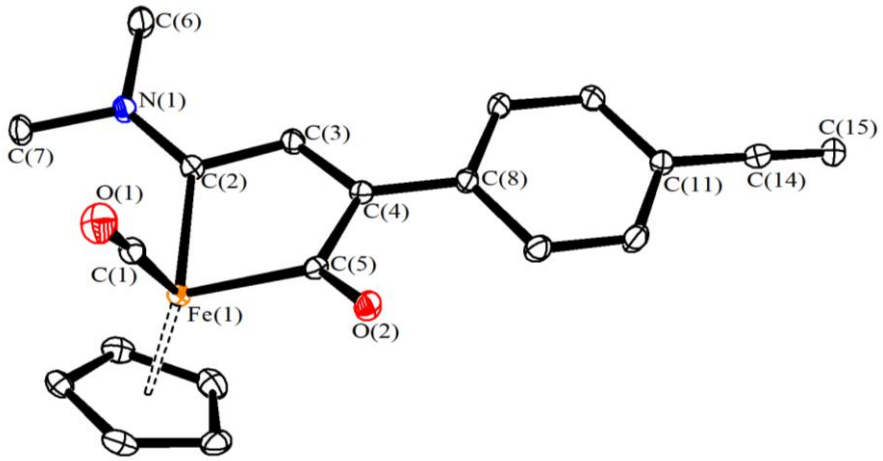

Figure 3. View of the structure of **4a1**. Displacement ellipsoids are at the 30% probability level. H-atoms have been omitted for clarity. Main bond distances (Å) and angles (°): Fe(1)-C(1) 1.7426(18), Fe(1)-C(2) 1.9261(17), Fe(1)-C(5) 1.9232(16), C(1)-O(1) 1.142(2), C(2)-N(1) 1.316(2), C(2)-C(3) 1.471(2), C(3)-C(4) 1.345(2), C(4)-C(5) 1.533(2), C(5)-O(2) 1.226(2), C(4)-C(8) 1.479(2), C(11)-C(14) 1.448(2), C(14)-C(15) , 1.181(3) Fe(1)-C(1)-O(1) 177.01(16), C(2)-Fe(1)-C(5) 81.95(7), Fe(1)-C(2)-C(3) 112.72(12), C(2)-C(3)-C(4) 115.17(15), C(3)-C(4)-C(5) 111.04(14), C(4)-C(5)-Fe(1) 112.06(11), C(11)-C(14)-C(15) 177.6(2), sum at N(1) 360.0(2).

To our delight, both **[1a^{ACN}]CF_3SO_3** and **[1b^{ACN}]CF_3SO_3** gave a smooth reaction with **4a1** in dichloromethane solution. Thus, the stable triiron products **[5a1]CF_3SO_3** and **[5b1]CF_3SO_3** were

cleanly obtained and subsequently isolated in 56-64% yields after purification through alumina column chromatography (Scheme 2).

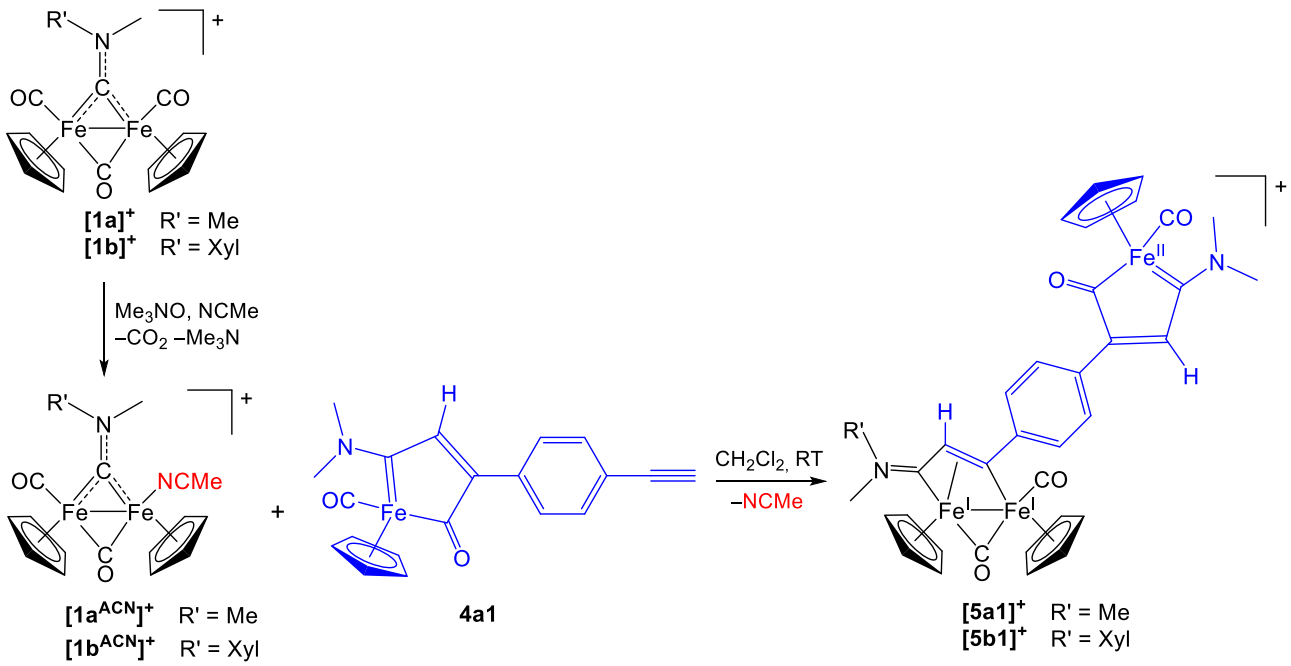

Scheme 2. Synthesis of mixed-valence triiron complexes by insertion of ferracyclic (Fe^{II}) alkynyl group into the iron-carbyne bond of diiron (Fe^{I} Fe^{I}) complexes. Triflate as counteranion for cationic complexes; Xyl = 2,6-$C_6H_3Me_2$.

The IR spectra of **[5a1]CF_3SO_3** and **[5b1]CF_3SO_3** in dichloromethane exhibit two bands accounting for the two carbonyl ligands belonging to the diiron core (e.g. at 1990 and 1811 cm^{-1} in [**5a1**]$^+$). They also include a band associated with the carbonyl ligand within the monoiron framework (1916 cm^{-1} in [**5a1**]$^+$).

The NMR spectra of **[5a1]CF_3SO_3** and **[5b1]CF_3SO_3** in acetone-d_6 consist of single sets of resonances. A comparative view of salient NMR data of **[5a1]CF_3SO_3** and **[5b1]CF_3SO_3**, alongside related complexes, is provided in the Supporting Information (Table S1). The possibility of isomerism due to the two potential geometries of the iminium substituents in [**5b1**]$^+$ (E-Z isomerism) has been ruled out. In fact, by comparing NMR data with those of the analogous complex $[Fe_2Cp_2(CO)(\mu\text{-}CO)\{\mu\text{-}\eta^1\text{:}\eta^3\text{-}C(Ph)CHC{=}NMe(Xyl)\}]^+$,[56] it has been determined that [**5b1**]$^+$ exists in solution exclusively in the E form. In other words, the xylyl ring points far away

from the Fe_2Cp_2 core. Ongoing from [**2a1**]$^+$ to **[5a1]**$^+$ / **[5b1]**$^+$, the resonances of the diiron scaffold experience only negligible shifts.

Some points deserve to be commented. First, the cooperativity of the diiron vinyliminium framework plays a central role. It is essential in providing easy access to the 5-membered ferracycle **4a1**, whose high degree of functionalization includes a pendant alkyne moiety. This alkyne, in turn, is exploited in the subsequent insertion process leading to the final triiron species. In other words, the C_3N chain within **4a1** is pre-constructed on the parent diiron compound. The cooperativity of the diiron vinyliminium assembly also enables the carbyne-alkyne coupling reaction involving three iron atoms. Another relevant point is that this reaction provides access to a polymetallic framework where the coordination environments around each metal significantly differ from each other. This differentiation forms the basis of the mixed valence nature of the triiron product. Besides, the bridging fragment within [**5a1**]$^+$ / [**5b1**]$^+$ can be described as the conjugation of vinyliminium and metallacyclic units through an aryl spacer and is unprecedented.

The structure of [**5a1**]$^+$ was optimized by DFT calculations (Figure 4). The computed geometrical parameters around Fe(1) closely resemble those experimentally measured for **4a1** (Figure 3), while the portion containing the diiron core (Fe2-Fe3) exhibits consistency with other similar bridged aminocarbyne complexes.[49]

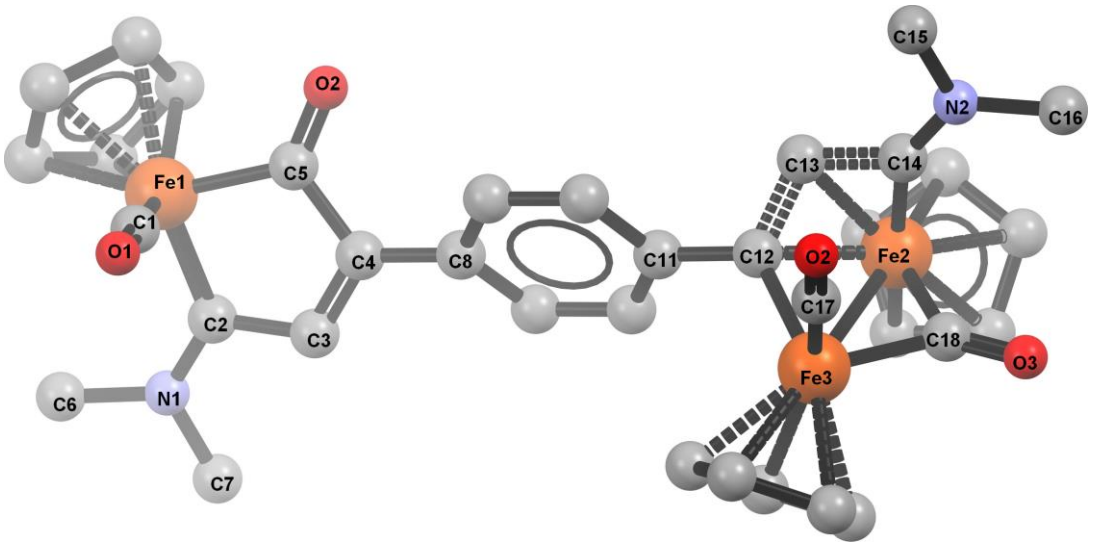

Figure 4. View of the DFT-optimized structure of [**5a1**]$^+$. Calculated bond distances (Å) and angles (°): Fe1-C1 1.743, Fe1-C2 1.908, Fe1-C5 1.945, C1-O1 1.165, C2-N1 1.346, C5-O2 1.219, C11-C12 1.475, C12-C13

1.428, C13-C14 1.424, Fe2-C12 2.050, Fe2-C13 2.046, Fe2-C14 1.832, C14-N2 1.306, Fe2-C18 1.948, Fe3-C12 1.970, Fe3-C18 1.879, C18-O3 1.184, Fe3-C17 1.741, C17-O2 1.161, Fe2-Fe3 2.570, Fe1-C1-O1 179.9, C2-Fe1-C5 87.3, sum at N1 359.9, Fe2-C12-Fe3 79.5, Fe3-C17-O2 178.6, Fe2-C18-Fe3 84.4, sum at N2 360.0. Hydrogens atoms are omitted for clarity.

The DFT-simulated infrared spectrum shows three characteristic peaks at 2020, 1996 and 1861 cm^{-1}, which nicely fits with the experimental ones at 1990, 1916 and 1811 cm^{-1}.

To gain a deeper insight into the properties and reactivity of [**5a1**]$^{+}$, we visualized the position of the highest occupied and the lowest unoccupied molecular orbitals (HOMO and LUMO, respectively). The HOMO is predominantly localized around Fe1, with a minor contribution from the Fe2-Fe3 moiety. Conversely, the LUMO shows the opposite distribution (Figure 5). It seems that the two sides of the complex are weakly interconnected.

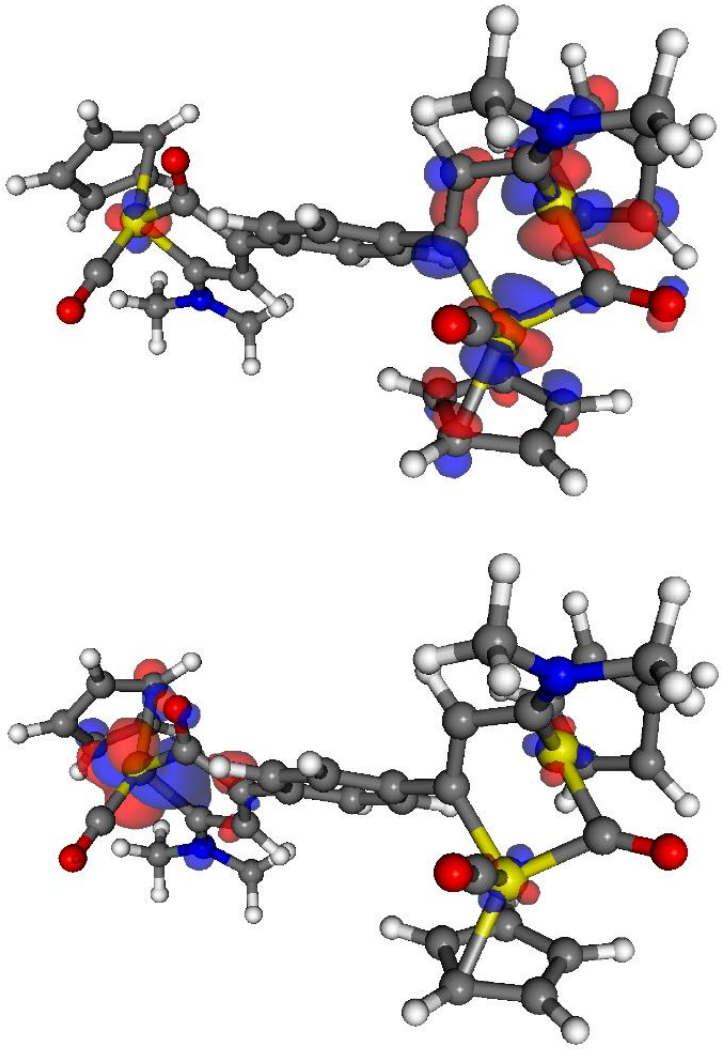

Figure 5. LUMO (up) and HOMO (down) orbitals of [**5a1**]$^{+}$.

The oxidation of [**5a1**]$^{+}$ to [**5a1**]$^{2+}$ (in a doublet state) results in subtle modification in the geometry of the complex. This includes the elongation of all coordination bonds around Fe1 and the shortening of C2-N1 and C5-O2 bonds (Figure S15). The moiety containing Fe2 and Fe3 is less affected, coherently with the localization of the HOMO in [**5a1**]$^{+}$.

Electrochemistry and IR spectroelectrochemistry

We studied the electrochemical and IR spectroelectrochemical behavior of **[5a1]CF$_3$SO$_3$** in CH_2Cl_2 solution containing $[N^nBu_4]PF_6$ as the electrolyte. To provide a basis for comparison, we also examined the precursor compound **4a1** and the diiron vinyliminium complex $[Fe_2Cp_2(CO)(\mu\text{-}CO)\{\mu\text{-}\eta^1\text{:}\eta^3\text{-}C(Ph)CHCNMe_2\}]CF_3SO_3$, **[6a]CF$_3SO_3$**, which shares a similar [Fe^{I}Fe^{I}] vinyliminium framework with **[5a1]CF$_3$SO$_3$**.

The cyclic voltammetry (CV) of **[5a1]CF$_3$SO$_3$** at a platinum electrode (Figure 6a) exhibits a mono-electron oxidation ($E°'$ = –0.15 V, ΔE_p = 75 mV), chemically reversible within the time scale of cyclic voltammetry; an irreversible oxidation is observed at higher potentials (E_p = +0.7 V). In the cathodic region, a two-electron reduction (E_p = –1.45 V) appears complicated by fast chemical reactions.

Similarly to other previously reported iron(II) vinyl-aminoalkylidene complexes,[56,68] **4a1** undergoes a mono-electron oxidation ($E°'$ = –0.14 V, ΔE_p = 70 mV) and a mono-electron reduction ($E°'$ = –1.86 V, ΔE_p = 80 mV). Both processes are diffusion controlled, displaying electrochemical and chemical reversibility (Figure 6b, orange line). We verified that the cationic complex [**6a**]$^{+}$, in $CH_2Cl_2/[N^nBu_4]PF_6$, experiences a mono-electron oxidation ($E°'$ = +0.66 V, ΔE_p = 75 mV), which is both electrochemically and chemically reversible. Additionally, [**6a**]$^{+}$ undergoes a two-electron reduction ($E°'$ = –1.35 V, ΔE_p = 60 mV) that is complicated due to subsequent chemical reactions (Figure 6b, green line). This behavior is in alignment with observations made with other compounds belonging to the family of [Fe^{I}Fe^{I}] vinyliminium complexes.[56]

Comparing the cyclovoltammetry profiles of **[5a1]CF_3SO_3**, **4a1** and **[6a]CF_3SO_3**, together with the formal potential values of their respective redox changes compiled in Table 1**,** it becomes evident that the processes of the mixed valence [$Fe^{I}Fe^{I}Fe^{II}$] complex result from the sum of those exhibited separately by its constituent parts (*i.e.*, [$Fe^{I}Fe^{I}$] and [Fe^{II}]). The oxidation of the cationic [**5a1**]$^+$ occurs at a potential almost identical to the oxidation of the neutral **4a1**, while the reduction potentials of [**5a1**]$^+$ and [**6a**]$^+$ are remarkably close. This data strongly suggests that the two iron-based redox systems, within the mixed valence triiron complex, remain independent despite the presence of the π-conjugated carbon bridge. This observation aligns with the DFT outcomes.

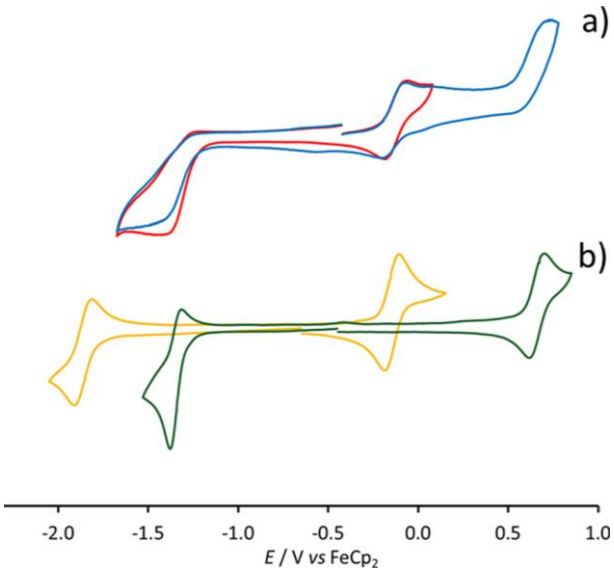

Figure 6. Cyclic voltammograms recorded at a Pt electrode in a CH_2Cl_2 solution of: a) **[5a1]CF_3SO_3** between −1.70 and +0.75 V (blue line), and between −1.70 and +0.05 V (red line); b) **4a1** (orange line) and **[6a]CF_3SO_3** (green line). [N^nBu_4]PF_6 (0.2 mol dm^{-3}) as supporting electrolyte. Scan rate: 0.1 V s^{-1}.

Table 1. Formal electrode potentials (V, *vs*. $FeCp_2$ and, in brackets, *vs*. Ag/AgCl) and peak-to-peak separations (mV) for the redox processes exhibited in CH_2Cl_2 solution by **[5a1]CF_3SO_3**, **4a1,** and **[6a]CF_3SO_3**.

Compound	Oxidation processes			Reduction process	
	$E°_1$	$E°_2$	$\Delta E_p{}^a$	$E°_3$	$\Delta E_p{}^a$
[5a1]CF_3SO_3	+0.70[b] (+1.15)	–0.15 (+0.30)	75	–1.45[b] (–1.00)	
4a1		–0.14 (+0.31)	70	–1.86 (–1.41)	80
[6a]CF_3SO_3		+0.66	75	–1.35	60

		(+1.11)		(–0.90)	

[a]Measured at 0.1 V/s. [b]Peak potential value for irreversible processes.

The *in situ* IR spectroelectrochemical (IR SEC) analysis of a $CH_2Cl_2/[N^nBu_4]PF_6$ solution of **[5a1]CF$_3$SO$_3$** provides further evidence for this finding. As the potential of the working electrode potential was gradually increased from –0.1 to +0.3 V (using a scan rate of 1 mV s^{-1}), only the 1916 cm^{-1} band of [**5a1**]$^+$ underwent a change: it was replaced by a new absorption at 2027 cm^{-1} (Figure 7). Notably, the two bands at 1990 and 1811 cm^{-1}, attributed to the terminal and bridging CO ligands within the [Fe^IFe^I frame], remained unchanged. For comparison, when examining the spectroelectrochemical oxidation of **4a1** (Figure S16), a fully reversible upshift of the terminal CO band (from 1916 cm^{-1} to 2029 cm^{-1}) was detected. The stability of the electrogenerated [**5a1**]$^{2+}$ in the time scale of the IR SEC experiment allowed a quantitative recovery of [**5a1**]$^+$ during the subsequent backward potential scan.

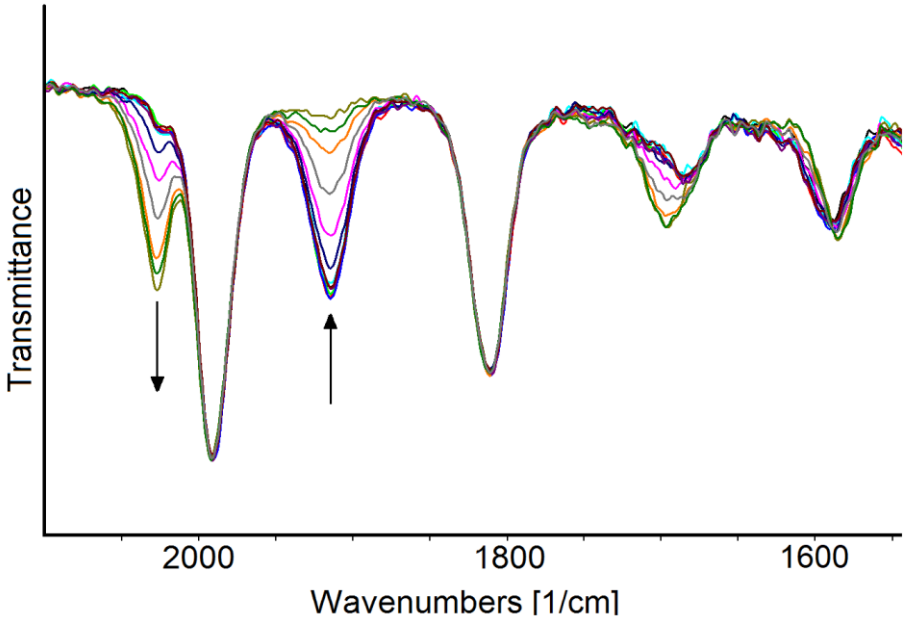

Figure 7. IR spectral changes of a CH_2Cl_2 solution of **[5a1]CF$_3$SO$_3$** recorded in an OTTLE cell during the progressive increase of the potential from –0.1 to +0.3 V (*vs*. Ag pseudoreference electrode). Scan rate 1.0 mV s^{-1}; spectra collected every minute. [N^nBu_4][PF_6] (0.2 mol dm^{-3}) as the supporting electrolyte. The absorptions of the solvent and supporting electrolyte have been subtracted.

When gradually decreasing the working electrode potential from –0.6 to –1.2 V (scan rate 2 mV s^{-1}), the two bands of [**5a1**]$^+$ at 1990 and 1811 cm^{-1} underwent a synchronized decrease in intensity. In their stead, a single absorption emerged, appearing as a shoulder of the 1916 cm^{-1} band (Figure 8a). The difference spectrum (Figure 8b, green line), generated by subtracting the initial spectrum from that obtained after the reduction, highlights a new absorption at 1885 cm^{-1}, while the 1916 cm^{-1} band remains unchanged.

Upon restoring the working electrode potential to its initial value during the backward oxidation step, the recovery of [**5a1**]$^+$ was only partial while a new band (at 1935 cm^{-1}) became evident in the difference spectrum (green line of Figure S17). The substitution of the two prominent absorptions at 1990 and 1811 cm^{-1} with a singular, moderately intense band at 1885 cm^{-1} upon reduction indicates a noteworthy and partially reversible reconfiguration of the [Fe^IFe^I] diiron framework. Interestingly, the band associated with the Fe^{II}-coordinated CO maintains its position and intensity without change during both the reduction and after partial decomposition. This observation points out a decomposition reaction reminiscent of the intramolecular rearrangement-fragmentation of [Fe^IFe^I] vinyliminium complexes, induced by reduction.[68]

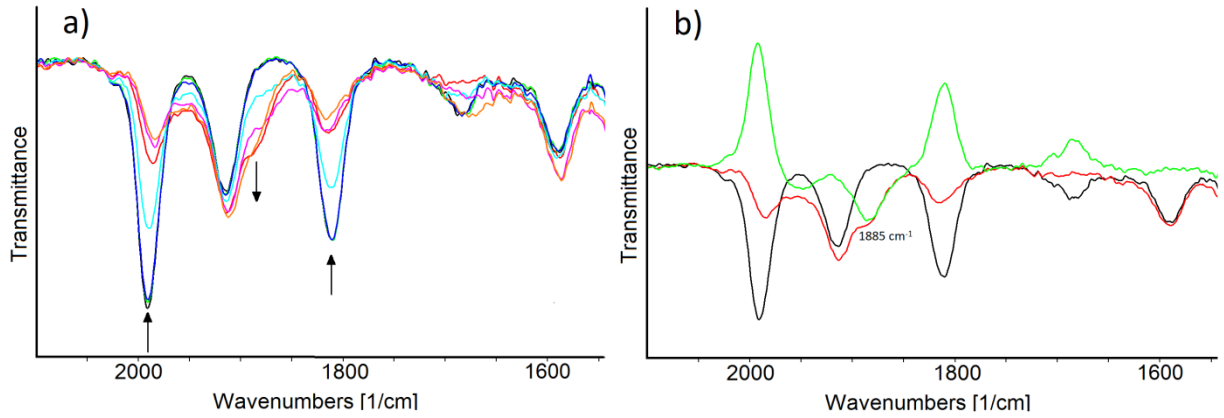

Figure 8. IR spectra of a CH_2Cl_2 solution of **[5a1]CF_3SO_3** recorded in an OTTLE cell a) during the progressive decrease of the potential from –0.6 to –1.2 V (*vs*. Ag pseudoreference electrode), scan rate 2.0 mV s^{-1}, spectra collected every minute.; b) initial spectrum (black line), at the WE potential of –1.2 V (red line) and difference spectrum (green line; red minus black). [N^nBu_4][PF_6] (0.2 mol dm^{-3}) as the supporting electrolyte. The absorptions of the solvent and supporting electrolyte have been subtracted.

Concluding remarks

The interest in developing new synthetic routes to access polynuclear complexes stems from the unique properties that these complexes may exhibit when compared to counterparts with lower nuclearity. Specifically, mixed valence complexes, which are based on metal centers displaying distinct oxidation states, have been intensively investigated. Their redox behavior is of interest to understand the potential role played by coordination linkers in the oxidation/reduction events. We have described a novel, room temperature and safe synthetic pathway that provides access to mixed valence triiron complexes. In these complexes, the iron atoms are separated by a novel and extensively functionalized unsaturated organic species, which acts as a multisite ligand. This specific ligand configuration ensures three distinct and robust coordination environments, a feature that is rarely observed, however electrochemical and DFT results evidence that the two metallic regions are not significantly interconnected during electron transfer processes.

Our synthetic approach exploits the cooperative effects within the $[Fe_2Cp_2(CO)_2]$ platform and contributes to the advancement of synthetic patterns involving earth abundant metal derivatives. Specifically, the iron-iron cooperativity enables two reaction pathways which would be otherwise not viable: 1) the clean transformation whereby an alkynyl-functionalized C_3 ligand (vinyliminium), bridging coordinated in a Fe_2 complex, is adapted to be included in a Fe_1 structure; 2) the coupling of such alkyne moiety with an aminocarbyne ligand on a Fe_2 complex. These two aspects and the easy application of this strategy can allow a future development of various trinuclear $[Fe^{I}Fe^{I}Fe^{II}]$ complexes with different substituents in both the dimeric and monomeric units. The ability to modify the nature of substituents can, in turn, enable the design and preparation of specific organo-iron compounds for biological applications, *e.g.* incorporating bioactive molecules.[69,70] Remarkably, the oxidation potential values exhibited by the trinuclear compound fall within the biologically relevant potential range, making the complex a promising candidate for future testing as a potential anticancer agent.

Experimental

Synthesis and characterization of complexes.

General details. Organic reactants (TCI Europe or Sigma Aldrich) were commercial products of the highest purity available. Complexes **[1a-b]CF_3SO_3** were prepared according to the literature.[71] Unless otherwise specified, synthesis and purification procedures were conducted in air. Once isolated, all products were stored in air. Dichloromethane and tetrahydrofuran were dried with the solvent purification system mBraun MB SPS5. Chromatography separations were carried out on columns of deactivated alumina (Sigma Aldrich, 4% *w/w* water) using solvents from the bottle. Infrared spectra of solutions were recorded on a Perkin Elmer Spectrum 100 FT-IR spectrometer with a CaF_2 liquid transmission cell (2300-1500 cm^{-1} range). IR spectra were processed with Spectragryph software.[72] NMR spectra were recorded at 298 K on a Jeol JNM-ECZ500R instrument equipped with a Royal HFX Broadband probe. Chemical shifts (expressed in parts per million) are referenced to the residual solvent peaks[73] (^1H, ^{13}C) or to external standards.[74] NMR spectra were assigned with the assistance of ^1H-^{13}C (*gs*-HSQC and *gs*-HMBC) correlation experiments.[75] Elemental analyses were performed on a Vario MICRO cube instrument (Elementar).

$[Fe_2Cp_2(CO)(\mu\text{-}CO)\{\mu\text{-}\eta^1\text{:}\eta^3\text{-}C^3(4\text{-}C_6H_4C{\equiv}CH)C^2HC^1NMe_2\}]CF_3SO_3$, [2a1]$CF_3SO_3$ (Figure 9).

Figure 9. Structure of **[2a1]**$^+$.

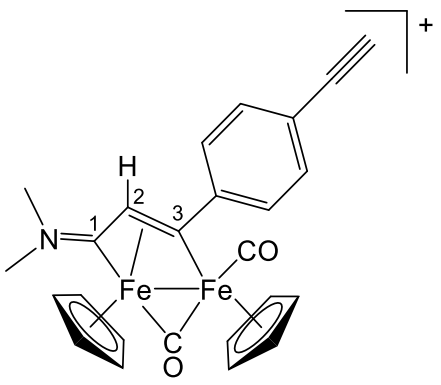

A solution of **[1a]CF_3SO_3** (275 mg, 0.518 mmol) in MeCN (15 mL) was treated with $Me_3NO{\cdot}2H_2O$ (63 mg, 0.57 mmol) and the resulting mixture was stirred for 1 hour, during which a progressive darkening of color was observed. The conversion of the starting material into the acetonitrile adduct was checked by IR spectroscopy [IR (CH_2Cl_2): $\tilde{\upsilon}/cm^{-1}$ = 1986vs (CO), 1816s (μ-CO), 1584m (μ-CN)], as is routine for this type of reaction.[76] Volatiles were removed under vacuum affording a brown residue, which was dissolved in CH_2Cl_2 (20 mL) and then treated with 1,4-diethynylbenzene (164 mg, 1.30 mmol). The mixture was stirred at room temperature for 48 hours and then the crude was charged on an alumina column. Thus, neat CH_2Cl_2 and THF were used to elute impurities, then a brown-red fraction corresponding to **[2a1]CF_3SO_3** was collected with MeCN/MeOH (9/1 v/v). Solvent evaporation afforded an oily residue. Dissolution into CH_2Cl_2 (ca. 5 mL) followed by pentane addition (ca. 30 mL) allowed to obtain a brown powdery precipitate, which was dried under vacuum. Yield 293 mg (90%). Anal. calcd. for $C_{26}H_{22}F_3Fe_2NO_5S$: C, 49.63; H, 3.52; N, 2.23; S, 5.10. Found: C, 49.55; H, 3.64; N, 2.12; S, 5.22. IR (CH_2Cl_2): $\tilde{\upsilon}/cm^{-1}$ = 2107w (C≡C), 1992vs (CO), 1808s (μ-CO), 1685m (C^1N). ^1H NMR (acetone-d_6): δ/ppm = 7.85, 7.64 (d, J = 8.3 Hz, 4 H, C_6H_4); 5.43, 5.28 (s, 10 H, Cp); 4.68 (s, 1 H, C^2H); 4.05, 3.47 (s, 6 H, NMe_2); 3.81 (s, 1 H, ≡CH). ^{13}C NMR (acetone-d_6): δ/ppm = 256.4 (μ-CO); 225.5 (C^1); 210.7 (CO); 202.2 (C^3); 157.6, 121.5 (*ipso*-C_6H_4); 132.7, 128.7 (C_6H_4); 92.4, 88.7 (Cp); 84.1 (<u>C</u>≡CH): 79.9 (C≡<u>C</u>H); 53.5 (C^2); 51.8, 45.0 (NMe_2).

[Fe_2Cp_2(CO)(μ-CO){μ-η^1:η^3-C^3((CH_2)$_3$C≡CH)$C^2HC^1NMe_2$}]CF_3SO_3, [2a2]CF_3SO_3 (Figure 10).

Figure 10. Structure of **[2a2]**$^+$.

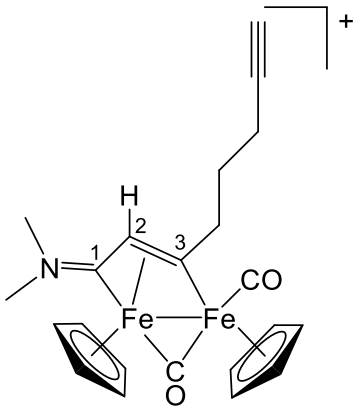

The titled compound was obtained by the same procedure used for the synthesis of **[2a1]CF_3SO_3**, from **[1a]CF_3SO_3** (290 mg, 0.546 mmol), $Me_3NO{\cdot}2H_2O$ (63 mg, 0.57 mmol) and 1,6-heptadiyne (0.16 mL, 1.4 mmol). Brown hygroscopic solid, yield 313 mg (96%). Anal. calcd. for $C_{23}H_{24}F_3Fe_2NO_5S$: C, 46.41; H, 4.06; N, 2.35; S, 5.39. Found: C, 46.55; H, 4.11; N, 2.29; S, 5.44. IR (CH_2Cl_2): $\tilde{\upsilon}/cm^{-1}$ = 2117w (C≡C), 1989vs (CO), 1805s (μ-CO), 1684m (C^1N). ^1H NMR (acetone-d_6): δ/ppm = 5.52, 5.21 (s, 10 H, Cp); 4.59 (s, 1 H, C^2H); 4.49, 3.9 (m, 2 H, C^3CH_2); 3.95, 3.33 (s, 6 H, NMe_2); 2.65-2.50 (m, 3 H, $C\underline{H_2}C{\equiv}C\underline{H}$); 2.39, 2.18 (m, 2 H, $CH_2C\underline{H_2}CH_2$). $^{13}C\{^1H\}$ NMR (acetone-d_6): δ/ppm = 257.4 (μ-CO); 226.7 (C^1); 212.3 (CO); 211.4 (C^3); 91.4, 88.4 (Cp); 85.0 ($\underline{C}{\equiv}CH$); 71.0 (≡CH); 54.2 ($C^3\underline{C}H_2$); 52.0 (C^2); 45.1 (NMe_2); 34.8 ($CH_2\underline{C}H_2CH_2$), 19.0 ($\underline{C}H_2C{\equiv}$). Crystals suitable for X-ray analysis were collected from slow diffusion of diethyl ether into a dichloromethane solution of **[2a2]CF_3SO_3**, at -30 °C.

$[Fe_2Cp_2(CO)(\mu\text{-}CO)\{\mu\text{-}\eta^1\text{:}\eta^3\text{-}C^3(4\text{-}C_6H_4C{\equiv}CH)C^2HC^1(CN)NMe_2\}]$, 3a1 (Figure 11).

Figure 11. Structure of **3a1**.

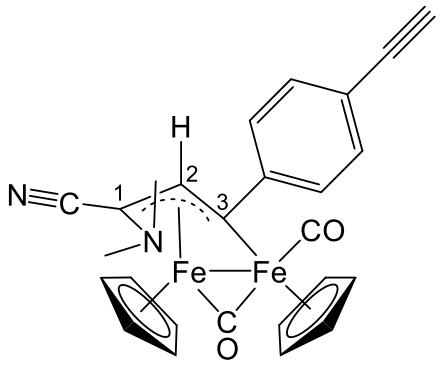

A solution of **[2a1]CF_3SO_3** (200 mg, 0.318 mmol) in anhydrous CH_2Cl_2 (20 mL) was treated with tetrabutylammonium cyanide (108 mg, 0.402 mmol), and this solution was stirred at room temperature for 1 hour under N_2 atmosphere. The final mixture was charged on an alumina column, and subsequent chromatography was carried out under N_2 atmosphere. Petroleum ether (40-60 °C) was used to elute impurities. Next, a brown-red fraction corresponding to **3a1** was collected using dichloromethane. Removal of the solvent under reduced pressure afforded a solid which was dissolved in the minimum volume of CH_2Cl_2; afterwards, addition of pentane (30-40 mL) allowed the precipitation of a dark-red powder, which was dried under vacuum and stored in air. Brown solid, yield 129 mg (80%). Anal. calcd. for $C_{26}H_{22}Fe_2N_2O_2$: C, 61.70; H, 4.38; N, 5.53. Found: C, 61.61; H, 4.29; N, 5.58. IR (CH_2Cl_2): $\tilde{\upsilon}/cm^{-1}$ = 2189m (C≡N), 2106vw (C≡C), 1970vs (CO), 1789s (μ-CO). ^1H NMR ($CDCl_3$): δ/ppm = 7.61, 7.60, 7.55 (m, 4 H, C_6H_4); 4.68, 4.61 (s, 10 H, Cp); 4.44 (s, 1 H, C^2H); 3.17 (s, 1 H, ≡CH); 2.35, 1.82 (s, 6 H, NMe_2). $^{13}C\{^1H\}$ NMR ($CDCl_3$): δ/ppm = 264.2 (μ-CO); 212.3 (CO); 198.5 (C^3); 159.9 (*ipso*-C_6H_4); 131.9, 127.7, 119.2 (C_6H_4); 120.8 (C≡N); 89.3, 86.1 (Cp); 83.8 (≡$\underline{C}$CH); 81.7 (C^2); 77.6 (≡C$\underline{C}$H); 64.9 (C^1); 49.8, 42.1 (NMe_2).

$[Fe_2Cp_2(CO)(\mu\text{-}CO)\{\mu\text{-}\eta^1\text{:}\eta^3\text{-}C^3((CH_2)_3C{\equiv}CH)C^2HC^1(CN)NMe_2\}]$, 3a2 (Figure 12).

Figure 12. Structure of **3a2**.

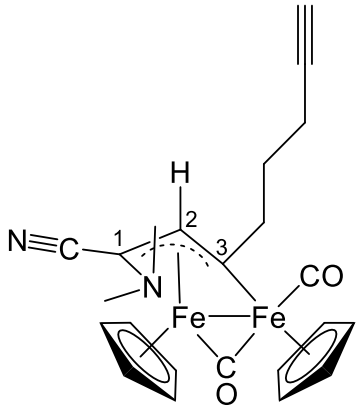

The titled compound was obtained by the same procedure used for the synthesis of **3a1**, from **[2a2]CF_3SO_3** (200 mg, 0.336 mmol) and tetrabutylammonium cyanide (105 mg, 0.391 mmol). Dark-red powder, yield 129 mg (81%). Anal. calcd. for $C_{23}H_{24}Fe_2N_2O_2$: C, 58.51; H, 5.12; N, 5.93. Found: C, 58.35; H, 5.20; N, 5.86. IR (CH_2Cl_2): $\tilde{\upsilon}/cm^{-1}$ = 2188m (C≡N), 2138w (C≡C), 1967vs (CO), 1788s (μ-CO). ^{1}H NMR ($CDCl_3$): δ/ppm = 4.88, 4.44 (s, 10 H, Cp); 4.38, 3.85 (m, 2 H, C^3CH_2); 4.34 (s, 1 H, C^2H), 2.62-2.56, 2.55-2.48 (m, 2 H, CH_2C≡); 2.40-2.32, 2.11-2.03 (m, 2 H, $CH_2CH_2CH_2$); 2.26, 1.69 (s, 6 H, NMe_2); 2.14 (t, 1 H, ≡CH). $^{13}C\{^1H\}$ NMR ($CDCl_3$): δ/ppm = 264.8 (μ-CO); 212.8 (CO); 204.8 (C^3); 121.1 (C≡N); 88.8, 86.0 (Cp); 84.6 (C≡CH); 82.3 (C^2); 69.5 (≡CH); 66.3 (C^1); 55.7 (C^3CH_2); 49.5 ($CH_2CH_2CH_2$); 42.2, 34.4 (NMe_2); 18.6 (CH_2C≡).

[Fe(Cp)(CO){C^1(NMe_2)C^2H=C^3(4-C_6H_4CCH)C(O)}], 4a1 (Figure 13).

Figure 13. Structure of **4a1**.

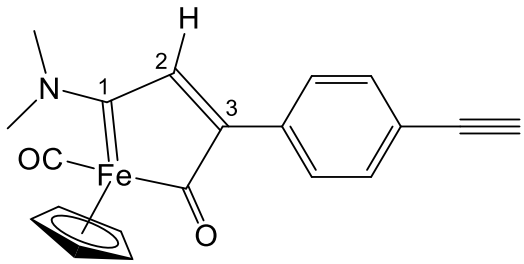

Compound **[2a2]CF_3SO_3** (200 mg, 0.318 mmol) was dissolved in anhydrous THF (25 mL), and pyrrolidine (0.78 mL, 30 eq.) was added. The mixture was left stirring for 72 hours under N_2

atmosphere, then volatiles were evaporated under reduced pressure. The solid residue was dissolved in dichloromethane and some alumina was added to this solution. After solvent removal under reduced pressure, the solid was charged on an alumina column and subsequent chromatography was performed under N_2 atmosphere. Petroleum ether (40-60°C) and petroleum ether/diethyl ether mixture (1/1 v/v) were used to elute impurities, then a brown-red band corresponding to the title product was collected with Et_2O/CH_2Cl_2 (1/1 v/v). Solvent evaporation allowed to collect **4a1** as a dark-red solid. Yield 54 mg (47%). Anal. calcd. for $C_{20}H_{17}FeNO_2$: C, 66.88; H, 4.77; N, 3.90. Found: C, 66.71; H, 4.89; N, 3.78. IR (CH_2Cl_2): $\tilde{\upsilon}/cm^{-1}$ = 2107vw (C≡C), 1916vs (CO), 1526m (C=O), 1602m (C^1N). ^1H NMR ($CDCl_3$): δ/ppm = 7.66 (s, 1 H, C^2H); 7.48 (m, 4 H, C_6H_4); 4.54 (s, 5 H, Cp); 3.74, 3.55 (s, 6 H, NMe_2); 3.13 (s, 1 H, ≡CH). $^{13}C\{^1H\}$ NMR ($CDCl_3$): δ/ppm = 270.2 (CO_{acyl}); 262.2 (C^1); 222.0 (CO); 168.5 (C^3); 146.7 (C^2); 133.3, 122.8 (*ipso*-C_6H_4); 132.1, 129.2 (C_6H_4); 85.4 (Cp); 83.8 (C≡CH); 78.6 (≡CH); 52.0, 43.4 (NMe_2). Crystals suitable for X-ray analysis were obtained from slow diffusion of pentane layered over a dichloromethane solution of **4a1**, at –30 °C.

$[Fe_2Cp_2(CO)(\mu\text{-}CO)\{\mu\text{-}\eta^1\text{:}\eta^3\text{-}C^3(4\text{-}C_6H_4C^4=C^5HC^6(NMe_2)=FeCp(CO)C=O)C^2HC^1NMe_2\}]CF_3SO_3$, $[5a1]CF_3SO_3$ (Figure 14).

Figure 14. Structure of **$[5a1]^+$**.

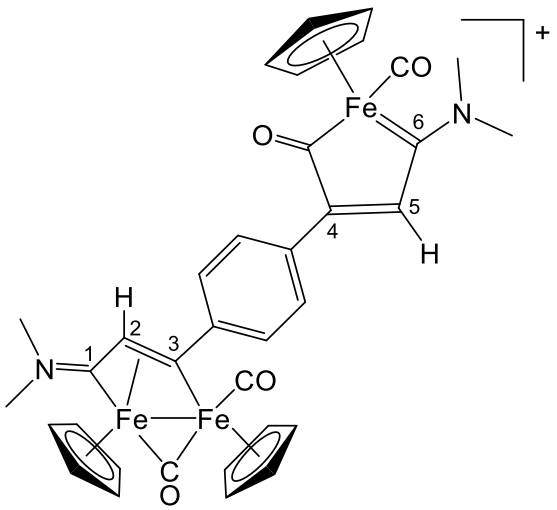

A solution of **4a1** (54 mg, 0.15 mmol) in CH_2Cl_2 (10 mL) was added to a solution in CH_2Cl_2 (10 mL) of **[1a^{ACN}]CF_3SO_3**, freshly prepared from **[1a]CF_3SO_3** (72 mg, 0.14 mmol) and $Me_3NO{\cdot}2H_2O$ (18 mg, 0.16 mmol), according to the procedure described for the synthesis of **[2a1]CF_3SO_3**. The mixture was stirred at room temperature for 48 hours, then it was charged on an alumina column. Elution with neat dichloromethane and CH_2Cl_2/THF (3/1 *v/v*) allowed to separate impurities, then a brown band corresponding to the title product was collected with MeCN/MeOH (9/1 *v/v*). Solvent evaporation under reduced pressure allowed to collect **[5a1]CF_3SO_3** as a brown solid. Yield 77 mg (64%). Anal. calcd. for $C_{36}H_{33}F_3Fe_3N_2O_7S$: C, 50.15; H, 3.86; N, 3.25; S, 3.72. Found: C, 50.25; H, 3.94; N, 2.12; S, 3.88. IR (CH_2Cl_2): $\tilde{\upsilon}$/cm^{-1} = 1990vs (CO), 1916s (CO), 1811s (μ-CO), 1674vw (C^1=N). ^{1}H NMR (acetone-d_6): δ/ppm = 8.14 (s, 1 H, C^5H); 7.84-7.78 (m, 4 H, C_6H_4); 5.42, 5.27 (s, 10 H, Fe_2Cp_2); 4.66 (s, 1 H, C^2H); 4.58 (s, 5 H, FeCp); 4.05, 3.47 (s, 6 H, C^1NMe_2); 3.85, 3.75 (s, 6 H, C^6NMe_2). ^{13}C NMR (acetone-d_6): δ/ppm = 268.3 (CO_{acyl}); 259.5 (C^6); 256.7 (μ-CO); 225.8 (C^1); 223.4 (FeCO); 210.8 (Fe_2CO); 203.4 (C^3); 168.2 (C^4); 157.7, 120.8 (*ipso*-C_6H_4); 147.9 (C^5); 130.1, 128.1 (C_6H_4); 92.5, 87.5 (Fe_2Cp_2); 85.9 (FeCp); 53.8 (C^2); 52.2, 45.0 ($C^1N\underline{Me}_2$); 51.8, 43.9 ($C^6N\underline{Me}_2$).

[Fe_2Cp_2(CO)(μ-CO){μ-η^1:η^3-C^3(4-$C_6H_4C^4$=C^5HC^6(NMeXyl)=FeCp(CO)C=O)$C^2HC^1NMe_2$}]CF_3SO_3, [5b1]CF_3SO_3 (Figure 15).

Figure 15. Structure of **[5b1]**$^+$.

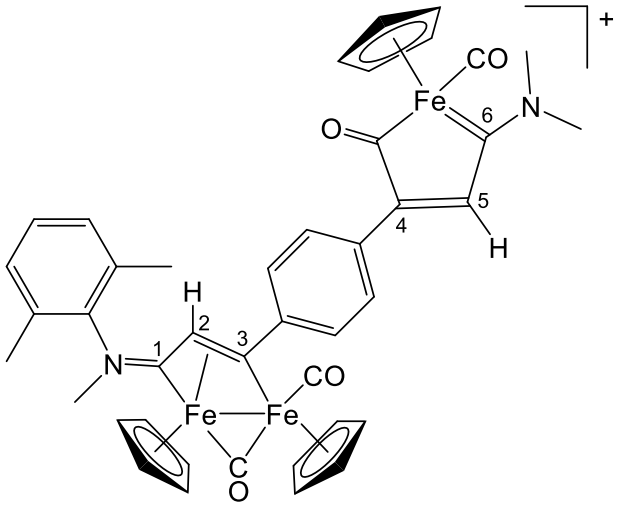

The title compound was obtained by the same procedure used for the synthesis of **[5a1]CF_3SO_3**, from **[1b]CF_3SO_3** (87 mg, 0.14 mmol), $Me_3NO{\cdot}2H_2O$ (19 mg, 0.17 mmol) and **4a1** (76 mg, 0.21 mmol). Chromatography: MeCN/MeOH (9/1 *v/v*). Brown solid, yield 74 mg (56%). Anal. calcd. for $C_{43}H_{39}F_3Fe_3N_2O_7S$: C, 54.23; H, 4.13; N, 2.94. Found: C, 54.15; H, 4.04; N, 3.02. IR (CH_2Cl_2): $\tilde{\upsilon}/cm^{-1}$ = 1989vs (CO), 1916s (CO), 1819vs (μ-CO), 1630 (C^1N), 1523 (C=O). ^1H NMR (acetone-d_6): δ/ppm = 8.11 (s, 1 H, C^5H); 7.75, 7.44-7.37, 7.26-7.22 (m, 7 H, C_6H_3 + C_6H_4); 5.18, 4.92 (s, 10 H, Fe_2Cp_2); 4.70 (s, 5 H, FeCp); 4.43 (s, 1 H, C^2H); 4.41 (s, 3 H, C^1NMe); 3.83, 3.71 (s, 6 H, C^6NMe_2); 2.33, 1.87 (s, 6 H, $C_6H_3\underline{Me_2}$). ^{13}C NMR (acetone-d_6): δ/ppm = 265.0 (CO_{acyl}); 259.5 (C^6); 254.4 (μ-CO); 233.1 (C^1); 223.4 (FeCO); 213.1 (Fe_2CO); 207.8 (C^3); 168.1 (C^4); 157.3 (*ipso*-C_6H_4); 147.9 (C^5); 146.3 (*ipso*-C_6H_3) 132.9-127.3 (C_6H_4 + C_6H_3); 93.3, 90.1 (Fe_2Cp_2); 85.8 (FeCp); 54.3 (C^2); 54.1, 43.8 ($C^6N\underline{Me_2}$); 46.3 ($C^1N\underline{Me}$); 18.8, 17.6 ($C_6H_3\underline{Me_2}$).

X-ray crystallography

Crystal data and collection details for **[2a2]CF_3SO_3** and **4a1** are reported in Table 2. Data were recorded on a Bruker APEX II diffractometer equipped with a PHOTON2 detector using Mo–Kα radiation. The structures were solved by direct methods and refined by full-matrix least-squares based on all data using F^2.[77] Hydrogen atoms were fixed at calculated positions and refined using a riding model.

Table 2. Crystal data and measurement details for **[2a2]CF_3SO_3** and **4a1**.

	[2a2]CF_3SO_3	**4a1**
Formula	$C_{23}H_{24}F_3Fe_2NO_5S$	$C_{20}H_{17}FeNO_2$
FW	595.19	359.20
T, K	100(2)	100(2)
λ, Å	0.71073	0.71073
Crystal system	Monoclinic	Monoclinic
Space group	$P2_1/c$	$P2_1/n$
a, Å	8.7756(5)	8.0498(13)
b, Å	18.6469(10)	15.316(3)
c, Å	14.7205(8)	13.650(2)
β,°	97.551(2)	100.963(10)
Cell Volume, Å^3	2837.9(2)	1652.2(5)
Z	4	4
D_c, g·cm^{-3}	1.656	1.444
μ, mm^{-1}	1.362	0.924
F(000)	1216	744
Crystal size, mm	0.24×0.21×0.14	0.19×0.18×0.15
θ limits,°	1.772-26.994	2.019-26.996
Reflections collected	32076	24938
Independent reflections	5097 [R_{int} = 0.0416]	3607 [R_{int} = 0.0286]
Data / restraints /parameters	5097 / 0 / 318	3607 / 0 / 219
Goodness on fit on F^2	1.229	1.103
R_1 ($I > 2\sigma(I)$)	0.0629	0.0310
wR_2 (all data)	0.1450	0.0764
Largest diff. peak and hole, e Å^{-3}	1.498 / –0.606	0.345 / –0.273

Electrochemistry and IR spectroelectrochemistry

Cyclic voltammetry measurements were performed with a PalmSens4 instrument interfaced to a computer employing PSTrace5 electrochemical software. Anhydrous CH_2Cl_2 (Merck) was stored under argon over 3Å molecular sieves. [N^nBu_4]PF_6 (Fluka, electrochemical grade) and $FeCp_2$ (Fluka) were used without further purification. CV measurements were carried out under argon using 0.2 M [N^nBu_4]PF_6 in CH_2Cl_2 as the supporting electrolyte. The working and the counter electrodes consisted of a Pt disk and a Pt gauze, respectively. A leakless miniature Ag/AgCl/KCl (3.4 mol/L) electrode (eDAQ) was employed as a reference. The three-electrode home-built cell was pre-dried by heating under vacuum and filled with argon. The Schlenk-type construction of the

cell maintained anhydrous and anaerobic conditions. The solution of supporting electrolyte, prepared under argon, was introduced into the cell and the CV of the solvent was recorded. The analyte was then introduced and voltammograms were recorded; lastly, a small amount of ferrocene was added, and the CV repeated. Under the present experimental conditions, the one-electron oxidation of ferrocene occurred at E° = +0.45 V *vs* Ag/AgCl, KCl (3.4 mol/L).

Hydrodynamic voltammetries with the renewal of the diffusion layer were obtained with a linear sweep voltammetry at a platinum disk rotating electrode (ν = 20 mV s^{-1} and ω = 1500 rpm) by using a Metrohom 628-10 rotating disk equipment.

Infrared (IR) spectroelectrochemical measurements were carried out using an optically transparent thin-layer electrochemical (OTTLE) cell equipped with CaF_2 windows, platinum mini-grid working and auxiliary electrodes and a silver wire pseudo-reference electrode.[78] During the microelectrolysis procedures, the electrode potential was controlled by a PalmSens4 instrument interfaced to a computer employing PSTrace5 electrochemical software. Argon-saturated CH_2Cl_2/$[N^nBu_4]PF_6$ 0.2 M solutions of the analyzed compound were used. The *in situ* spectroelectrochemical experiments were performed by collecting IR spectra at fixed time intervals during oxidation or reduction, obtained by continuously increasing or lowering the initial working potential at a scan rate of 1.0 or 2.0 mV s^{-1}.

DFT calculations

All geometries were optimized with ORCA 4.2.0 using the B97 functional[79] in conjunction with a def2-sVP, while the properties have been computed by using the def2-tzVP basis set.[80] The effect of the solvent has been simulated through the continuum-like polarizable continuum model (C-PCM, dichloromethane). The dispersion corrections were introduced using the Grimme D3-parametrized correction and the Becke Johnson damping to the DFT energy.[81] All structures were confirmed to be local energy minima (no imaginary frequencies).

Author contributions

G.B.: synthesis and characterization of compounds, data analysis and writing; G.C.: DFT calculations, and writing; S.Z.: X-ray studies, and writing; S.S.: synthesis and characterization of compounds; G.P.: funding and supervision; T.F.: electrochemical and spectroelectrochemical studies, data analysis and writing; F.M.: data analysis, funding, and supervision.

Acknowledgements

We thank the University of Pisa for financial support (Fondi di Ateneo 2021).

Supporting Information Available

NMR spectra and comparison of data (Figures S1-S14 and Table S1); DFT and spectroelectrochemical results (Figures S15-S17). CCDC reference numbers 2289786 (**[2a2]CF_3SO_3**) and 2289787 (**4a1**) contain the supplementary crystallographic data for the X-ray studies reported in this work. These data are available free of charge at http://www.ccdc.cam.ac.uk/structures.

The authors declare no competing financial interests.

References

1 N. Svahn, A. J. Moro, C. Roma-Rodrigues, R. Puttreddy, K. Rissanen, P. V. Baptista, A. R. Fernandes, J. Carlos Lima, L. Rodríguez, The important role of the nuclearity, rigidity and solubility of phosphane ligands on the biological activity of gold(I) complexes, Chem. Eur. J. 2018, 24, 14654-14667.

2 T. M. Powers, T. A. Betley, Testing the Polynuclear Hypothesis: Multielectron Reduction of Small Molecules by Triiron Reaction Sites, J. Am. Chem. Soc. 2013, 135, 12289 – 12296.

3 M. Reiners, D. Baabe, K. Münster, M.-K. Zaretzke, M. Freytag, P. G. Jones, Y. Coppel, S. Bontemps, I. del Rosal, L. Maron, M. D. Walter, NH_3 formation from N2 and H2 mediated by molecular tri-iron complexes, Nat. Chem. 2020, 12, 740–746.

4 J. T. Hupp, Mixed Valence Dinuclear Species, in Compr. Coord. Chem. II, 2004, vol. 2, pp. 709-716.

5 D. F. Watson, A. B. Bocarsly, The effects of electronic coupling and solvent broadening on the intervalent electron transfer of a centrosymmetric mixed-valence complex, Coord. Chem. Rev. 2001, 211, 177–194.

6 K. Costuas, S. Rigaut, Polynuclear carbon-rich organometallic complexes: clarification of the role of the bridging ligand in the redox properties, Dalton Trans., 2011, 40 , 5643–5658.

7 S. Naik, S. Ø. Scottwell, H. L. Li, C. F. Leong, D. M. D'Alessandro, L. D. Field, Dinuclear acetylide-bridged ruthenium(ii) complexes with rigid non-aromatic spacers, Dalton Trans., 2020, 49, 2687-2695.

8 B. A. Etzenhouser, M. Di Biase Cavanaugh, H. N. Spurgeon, M. B. Sponsler, Mixed-Valence Diiron Complexes with Butadienediyl Bridges, J. Am. Chem. Soc. 1994, 116, 2221-2222.

9 R. Liyanage, Q. Yang, M. Fang, D. Li, J. Y. Lu, A μ3-oxo-centered mixed-valence triiron coordination polymer constructed by 5-bromonicotinato ligands, Inorg. Chem. Commun. 2018, 92, 121–124.

10 M. A. Andrews, H. D. Kaesz, Synthesis of Triiron Carbonyl Cluster Complexes Containing Isomeric Triply Bridging Acimidoyl or Alkylidenimido Group Derived from the Reduction of Organic Nitriles, J. Am. Chem. Soc. 1979, 7238-7244.

11 T. Kajiwara, T. Ito, Mixed-Valent Heptairon Complex with a Ground-State Spin Value of S = 12/2 Constructed from a Triiron Cluster Ligand, Angew. Chem. 2000, 112, 1.

12 A. M. Bond, R. J. H. Clark, D. G. Humphrey, P. Panayiotopoulos, B. W. Skelton, A. H. White, Synthesis, characterisation and electrochemical reductions of oxo-centred, carboxylate-bridged triiron complexes, J. Chem. Soc., Dalton Trans. 1998, 1845–1852.

13 R. B. Ferreira, L. J. Murray, Cyclophanes as Platforms for Reactive Multimetallic Complexes, Acc. Chem. Res. 2019, 52, 447−455

14 G. L. Guillet, K. Y. Arpin, A. M. Boltin, J. B. Gordon, J. A. Rave, P. C. Hillesheim, Synthesis and Characterization of a Linear Triiron(II) Extended Metal Atom Chain Complex with Fe-Fe bonds, Inorg. Chem. 2020, 59, 11238 − 11243

15 C. Dfaz, A. Arancibia, The cyanide ligand as an efficient bridge in mixed-valence complexes, lnorg. Chim. Acta 1998, 269, 246—252.

16 L. Biancalana, G. Bresciani, C. Chiappe, F. Marchetti, G. Pampaloni, C. S. Pomelli, Modifying bis(triflimide) ionic liquids by dissolving early transition metal carbamates, Phys. Chem. Chem. Phys., 2018, 20, 5057-5066.

17 W. Bonrath, K. R. Porschke, G. Wilke, K. Angermund, and C. Knuger, Mono-and Dinuclear Nickel (0) Complexes of Butadiyne, Angew. Chem. Int. Ed. 1988, 27, 833–835.

18 M. L. Buil and M. A. Esteruelas, Synthesis and Characterization of Ruthenium−Osmium Complexes Containing μ-Bisalkenyl, μ-Alkenylvinylidene, and μ-Alkenylcarbene Bridge Ligands, Organometallics 1999, 18, 1798–1800.

19 C.-K. Wong, G.-L. Lu, C.-L. Ho, W.-Y. Wong, Z. Li, Synthesis, Characterization and Structural Properties of Some Heterobimetallic Carbonyl Clusters Derived from Diethynylsilane and Diethynyldisilane Ligands, J. Cluster Sci. 2012, 23, 885–900.

20 R. D. Adams, B. Qu, M. D. Smith, T. A. Albright, Syntheses, Structures, Bonding, and Redox Behavior of 1,4-Bis(ferrocenyl)butadiyne Coordinated Osmium Clusters, Organometallics 2002, 21, 2970–2978.

21 M. Akita, M. Terada, M. Tanaka, Y. Morooka, Interaction of iron ethynyl and ethynediyl complexes with $Cp_2Ni_2(CO)_2$: formation of tri- and tetranuclear adducts with a multiply bridging C_2H ligand, Organometallics 1992, 11, 10, 3468–3472.

22 R. D. Adams, The Insertion of Alkynes into Metal-Metal Bonds and Organic Chemistry of the Dimetallated Olefin Complexes, Chem. Soc. Rev. 1994, 335-339.

23 R. B. Bedford, C. S.J. Cazin, Alkyne insertion reactions of $[RuH(\kappa^2\text{-}S_2CNEt_2)(CO)(PPh_3)_2]$: synthesis of alkenyl, alkynyl and enynyl complexes, J. Organomet. Chem. 2000, 598, 20–23.

24 I. Jourdain, M. Knorr, C. Strohmann, C. Unkelbach, S. Rojo, P. Gómez-Iglesias, F. Villafañe, Reactivity of Silyl-Substituted Iron − Platinum Hydride Complexes toward Unsaturated Molecules: 4. Insertion of Fluorinated Aromatic Alkynes into the Platinum − Hydride Bond. Synthesis and Reactivity of Heterobimetallic Dimetallacylopentenone, Dimetallacyclobutene, μ- Vinylidene, and μ 2 -σ -Alkenyl Complexes, Organometallics 2013, 32, 5343 − 5359

25 P- M. Jurd, H. L. Li, M. Bhadbhade, J. D. Watson, L. D. Field, Ferralactone formation from iron acetylides and carbon dioxide, J. Organomet. Chem. 961, 122252.

26 Y. Luo, X. Pan, X. Yu, J. Wu, Double carbometallation of alkynes: an efficient strategy for the construction of polycycles, Chem. Soc. Rev., 2014, 43, 834—846.

27 G. Bresciani, S. Boni, T. Funaioli, S. Zacchini, G. Pampaloni, N. Busto, T. Biver, F. Marchetti, Adding Diversity to a Diruthenium Biscyclopentadienyl Scaffold via Alkyne Incorporation: Synthesis and Biological Studies, Inorg. Chem. 2023, 62, 12453−12467.

28 A. S. Mohamed, I. Jourdain, M. Knorr, S. Boullanger, L. Brieger, C. Strohmann, Heterodinuclear Diphosphane-Bridged Iron–Platinum Diyne Complexes as Metalloligands for the Assembly of Polymetallic Systems (Fe, Pt, Co), J. Clu. Sci. 2019, 30, 1211–1225.

29 S. Rana, J. Prasad Biswas, S. Paul, A. Paik, D. Maiti, Organic synthesis with the most abundant transition metal–iron: from rust to multitasking catalysts, Chem. Soc. Rev. 2021, 50, 243-472.

30 A. Fürstner, Iron Catalysis in Organic Synthesis: A Critical Assessment of What It Takes To Make This Base Metal a Multitasking Champion, ACS Cent. Sci. 2016, 2, 778 – 789.

31 Y. Wang, J. Zhu, A. C. Durham, H. Lindberg, Y.-M. Wang, α-C−H Functionalization of π- Bonds Using Iron Complexes: Catalytic Hydroxyalkylation of Alkynes and Alkenes, J. Am. Chem. Soc. 2019, 141, 19594−19599.

32 J. T. Kleinhaus, F. Wittkamp, S. Yadav, D. Siegmund, U.-P. Apfel, [FeFe]-Hydrogenases: maturation and reactivity of enzymatic systems and overview of biomimetic models, Chem. Soc. Rev., 2021, 50, 1668-1784.

33 S. Gupta Sreerama, S. Pal, A Triiron Complex Containing the Carboxylate-Free $\{Fe_3(\mu_3\text{-}O)\}_7$ Core and Distorted Pentagonal-Bipyramidal Metal Centres, Eur. J. Inorg. Chem. 2004, 4718 4723

34 L. Marchi, S. Carlino, C. Castellano, F. Demartin, A. Forni, A. M. Ferretti, A. Ponti, A. Pasini, L. Rigamonti, Substituent-Guided Cluster Nuclearity for Tetranuclear Iron(III) Compounds with Flat $\{Fe_4(\mu_3\text{-}O)_2\}$ Butterfly Core, Int. J. Mol. Sci. 2023, 24, 5808

35 T. M. Powers, A. R. Fout, S.L. Zheng, T. A. Betley, Oxidative Group Transfer to a Triiron Complex to Form a Nucleophilic μ3-Nitride, $[Fe_3(\mu_3\text{-}N)]$-, J. Am. Chem. Soc. 2011, 133, 3336 – 3338.

36 A. Rahaman, S. Ghosh, D. G. Unwin, S. Basak-Modi, K. B. Holt, S. E. Kabir, E. Nordlander, M. G. Richmond, G. Hogarth, Bioinspired Hydrogenase Models: The Mixed-Valence Triiron Complex $[Fe_3(CO)_7(\mu\text{-edt})_2]$ and Phosphine Derivatives $[Fe_3(CO)_{7-x}(PPh_3))_x(\mu\text{-edt})_2]$ (x = 1, 2) and $[Fe_3(CO)_5(\kappa2\text{-diphosphine})(\mu\text{-edt})_2]$ as Proton Reduction Catalysts, Organometallics 2014, 33, 1356 – 1366.

37 S. Ghosh, G. Hogarth, K. B. Holt, S. E. Kabir, A. Rahaman, D. G. Unwin, Bio-inspired hydrogenase models: mixed-valence triion complexes as proton reduction catalysts, Chem. Commun. 2011, 47 , 11222–11224.

38 J. M. Camara, T. B. Rauchfuss, Combining acid–base, redox and substrate binding functionalities to give a complete model for the [FeFe]-hydrogenase, Nat. Chem. 2012, 4, 26-30.

39 C. Tard, X. Liu, D. L. Hughes and C. J. Pickett, A novel {FeI–FeII–FeII–FeI} iron thiolate carbonyl assembly which electrocatalyses hydrogen evolution, Chem. Commun., 2005, 133-135.

40 V. Ritleng, M. J. Chetcuti, Hydrocarbyl Ligand Transformations on Heterobimetallic Complexes, Chem. Rev. 2007, 107, 797−858.

41 F. Y. Pétillon, P. Schollhammer, J. Talarmin, Recent advances in the chemistry of tris(thiolato) bridged cyclopentadienyl dimolybdenum complexes, Coord. Chem. Rev. 2017, 331, 73–92.

42 C. B. van Beek, N. P. van Leest, M. Lutz, S. D. de Vos, R. J. M. Klein Gebbink, B. de Bruin, D. L. J. Broere, Combining metal–metal cooperativity, metal–ligand cooperativity and chemical non-innocence in diiron carbonyl complexes, Chem. Sci. 2022, 13, 2094 – 2104.

43 R. Govindarajan, S. Deolka, J. R. Khusnutdinova, Heterometallic bond activation enabled by unsymmetrical ligand scaffolds: bridging the opposites, Chem. Sci. 2022, 13, 14008-14031.

44 M. Knorr, I. Jourdain, A. Said Mohamed, A. Khatyr, S. G. Koller, C. Strohmann, Synthesis and reactivity of bis(diphenylphosphino)amine-bridged heterobimetallic ironeplatinum m-isonitrile and m-aminocarbyne complexes, J. Organomet. Chem. 2015, 780, 70-85.

45 H. Tsurugi, P. Laskar, K. Yamamoto, K. Mashima, Bonding and structural features of metal-metal bonded homo- and hetero-dinuclear complexes supported by unsaturated hydrocarbon ligands, J. Organomet. Chem. 2018, 869, 251-263.

46 M. Knorr, I. Jourdain, Activation of alkynes by diphosphine- and μ-phosphido-spanned heterobimetallic complexes, Coord. Chem. Rev. 2017, 350, 217–247.

47 T. S. Piper, F. A. Cotton, G. Wilkinson, Cyclopentadienyl-Carbon Monoxide and Related Compounds of Some Transitional Metals, J. Inorg. Nucl. Chem., 1955, 1, 165–174.

48 L. Busetto, P. M. Maitlis, V. Zanotti, Bridging vinylalkylidene transition metal complexes, Coord. Chem. Rev. 2010, 254, 470–486.

49 L. Biancalana, F. Marchetti, Aminocarbyne ligands in organometallic chemistry, Coord. Chem. Rev. 2021, 449, 214203.

50 Mazzoni, R.; Salmi, M.; Zanotti, V. C-C Bond Formation in Diiron Complexes. Chem. Eur. J. 2012, 18, 10174-10194

51 G. Bresciani, S. Schoch, L. Biancalana, S. Zacchini, M. Bortoluzzi, G. Pampaloni, F. Marchetti, Cyanide–Alkene Competition in a Diiron Complex and Isolation of a Multisite (Cyano)Alkylidene–Alkene Species, Dalton Trans., 2022, 51, 1936–1945.

52 Wadepohl, H.; Gebert, S.; Pritzkow, H.; Osella, D.; Nervi, C.; Fiedler, J. Redox Chemistry of $[Co_4(CO)_3(\mu_3\text{-}CO)_3(\mu_3\text{-}C_7H_7)(\eta^5\text{-}C_7H_9)]$ – Reversible Carbon−Carbon Coupling versus Metal Cluster Degradation, Eur. J. Inorg. Chem. 2000, 1833-1843.

53 Casey, C. P.; Austin, E. A.; Rheingold, A. L. Reaction of diiron .mu.-alkylidyne complexes with diazo compounds, Organometallics 1987, 6, 2157-2164.

54 G. Agonigi, L. K. Batchelor, E. Ferretti, S. Schoch, M. Bortoluzzi, S. Braccini, F. Chiellini, L. Biancalana, S. Zacchini, G. Pampaloni, B. Sarkar, P. J. Dyson, F. Marchetti, Mono-, Di- and Tetra-iron Complexes with Selenium or Sulphur Functionalized Vinyliminium Ligands: Synthesis, Structural Characterization and Antiproliferative Activity, Molecules 2020, 25, 1656.

55 F. Marchetti, Constructing Organometallic Architectures from Aminoalkylidyne Diiron Complexes, Eur. J. Inorg. Chem., 2018, 3987–4003.

56 Rocco, D.; Batchelor, L. K.; Agonigi, G.; Braccini, S.; Chiellini, F.; Schoch, S.; Biver, T.; Funaioli, T.; Zacchini, S.; Biancalana, L.; Ruggeri, M.; Pampaloni, G.; Dyson, P. J.; Marchetti, F. Anticancer Potential of Diiron Vinyliminium Complexes. Chem. Eur. J. 2019, 25, 14801-14816.

57 Luh, T.-Y. Trimethylamine N-Oxide-A Versatile Reagent For Organometallic Chemistry. Coord. Chem. Rev. 1984, 60, 255-276.

58 Alvarez, M. A.; García, M. E.; García-Vivó, D.; Huergo, E.; Ruiz, M. A. Acetonitrile Adduct [MoReCp(μ-H)(μ-PCy_2)$(CO)_5$(NCMe)]: A Surrogate of an Unsaturated Heterometallic Hydride Complex, Inorg. Chem. 2018, 57, 912−915.

59 G. Bresciani, S. Zacchini, G. Pampaloni, F. Marchetti, Carbon–Carbon Bond Coupling of Vinyl Molecules with an Allenyl Ligand at a Diruthenium Complex, Organometallics 2022, 41, 1006-1014.

60 B. Campanella, S. Braccini, G. Bresciani, M. De Franco, V. Gandin, F. Chiellini, A. Pratesi, G. Pampaloni, L. Biancalana, F. Marchetti, The choice of μ-vinyliminium ligand substituents is key to optimize the antiproliferative activity of related diiron complexes, Metallomics 2023, 15, mfac096.

61 L. Busetto, P. M. Maitlis, V. Zanotti, Bridging vinylalkylidene transition metal complexes, Coord. Chem. Rev. 2010, 254, 470–486.

62 S. G. Eaves, D. S. Yufit, B. W. Skelton, J. A. K. Howard, P. J. Low, Syntheses, structural characterisation and electronic structures of some simple acyclic amino carbene complexes, Dalton Trans., 2015,44, 14341-14348.

63 Ciancaleoni, G.; Zacchini, S.; Zanotti, V.; Marchetti, F. DFT Mechanistic Insights into the Alkyne Insertion Reaction Affording Diiron μ-Vinyliminium Complexes and New Functionalization Pathways. Organometallics. 2018, 37, 3718-3731.

64 S. Schoch, L. K. Batchelor, T. Funaioli, G. Ciancaleoni, S. Zacchini, S. Braccini, F. Chiellini, T. Biver, G. Pampaloni, P. J. Dyson and F. Marchetti, Diiron Complexes with a Bridging Functionalized Allylidene Ligand: Synthesis, Structural Aspects, and Cytotoxicity. Organometallics, 2020, 39, 361-373.

65 F. Thetiot, S. Triki, J. S. Pala, Polynitriles as ligands: new coordination polymers with the 1,1,3,3-tetracyano-2-ethoxypropenide (tcnp−) bridging ligand, Polyhedron 2003, 22, 1837-1843.

66 D. Rocco, L. K. Batchelor, E. Ferretti, S. Zacchini, G. Pampaloni, P. J. Dyson, F. Marchetti, Piano Stool Aminoalkylidene-Ferracyclopentenone Complexes from Bimetallic Precursors: Synthesis and Cytotoxicity Data, ChemPlusChem 2020, 85, 110–122.

67 G. Bresciani, S. Zacchini, G. Pampaloni, M. Bortoluzzi, F. Marchetti, Diiron Aminocarbyne Complexes with NCE− Ligands (E = O, S, Se), Molecules 2023, 28, 3251.

68 G. Agonigi, G. Ciancaleoni, T. Funaioli, S. Zacchini, F. Pineider, C. Pinzino, G. Pampaloni, V. Zanotti, F. Marchetti, Controlled Dissociation of Iron and Cyclopentadienyl from a Diiron Complex with a Bridging C_3 Ligand Triggered by One-Electron Reduction, Inorg. Chem. 2018, 57, 15172−15186.

69 S. Schoch, M. Hadiji, S.A.P. Pereira, M. L. M. F. S. Saraiva, S. Braccini, F. Chiellini, T. Biver, S. Zacchini, G. Pampaloni, P. J. Dyson, F. Marchetti, A Strategy to Conjugate Bioactive Fragments to Cytotoxic Diiron Bis(cyclopentadienyl) Complexes, Organometallics, 2021, 40, 15, 2516-2528.

70 B. Campanella, S. Braccini, G. Bresciani, M. De Franco, V. Gandin, F. Chiellini, A. Pratesi, G. Pampaloni, L. Biancalana, F. Marchetti, The choice of μ-vinyliminium ligand substituents is key to optimize the antiproliferative activity of related diiron complexes, Metallomics, 15, 1, mfac096

71 G. Agonigi, M. Bortoluzzi, F. Marchetti, G. Pampaloni, S. Zacchini and V. Zanotti. Additions to Diiron Carbonyl Complexes Containing a Bridging Aminocarbyne Ligand: A Synthetic, Crystallographic and DFT Study. Eur. J. Inorg. Chem. 2018, 960–971.

72 F. Menges, "Spectragryph - optical spectroscopy software", Version 1.2.5, @ 2016-2017, http://www.effemm2.de/spectragryph.

73 G. R. Fulmer, A. J. M. Miller, N. H. Sherden, H. E. Gottlieb, A. Nudelman, B. M. Stoltz, J. E. Bercaw, K. I. Goldberg, NMR Chemical Shifts of Trace Impurities: Common Laboratory Solvents, Organics, and Gases in Deuterated Solvents Relevant to the Organometallic Chemist, Organometallics 2010, 29, 2176–2179.

74 R. K. Harris, E. D. Becker, S. M. Cabral De Menezes, R. Goodfellow, P. Granger, NMR nomenclature. Nuclear spin properties and conventions for chemical shifts (IUPAC Recommendations 2001), Pure Appl. Chem. 2001, 73, 1795–1818.

75 W. Willker, D. Leibfritz, R. Kerssebaum, W. Bermel, Gradient selection in inverse heteronuclear correlation spectroscopy, Magn. Reson. Chem. 1993, 31, 287-292.

76 Albano, V. G.; Busetto, L.; Monari, M; Zanotti, V.; Reactions of acetonitrile di-iron μ-aminocarbyne complexes; synthesis and structure of $[Fe_2(\mu\text{-}CNMe_2)(\mu\text{-}H)(CO)_2(Cp)_2]$, J. Organomet. Chem. 2000, 606, 163–168.

77 Sheldrick, G. M. Crystal structure refinement with SHELXL. Acta Crystallogr. C2015, 71, 3-8.

78 M. Krejčik, M. Daněk and F. Hartl, Simple construction of an infrared optically transparent thin-layer electrochemical cell: Applications to the redox reactions of ferrocene, $Mn_2(CO)_{10}$ and $Mn(CO)_3$(3,5-di-t-butyl-catecholate), J. Electroanal. Chem., 1991, 317, 179–187.

79 Becke, A. D. Density-functional thermochemistry. V. Systematic optimization of exchange-correlation functionals. J. Chem. Phys. 1997, 107, 8554-8560.

80 Weigend, F. Accurate Coulomb-fitting basis sets for H to Rn. Phys. Chem. Chem. Phys. 2006, 8, 1057−1065.

81 Grimme, S. Semiempirical GGA-type density functional constructed with a long-range dispersion correction. J. Comput. Chem. 2006, 27, 1787−1789.